Magnetoviscosity of semidilute ferrofluids and the role of dipolar interactions: Comparison of molecular simulations and dynamical mean-field theory

Patrick Ilg,[1,*] Martin Kröger,[2] and Siegfried Hess[1]
[1]*Institut für Theoretische Physik, Technische Universität Berlin, Hardenbergstrasse 36, D-10623 Berlin, Germany*
[2]*Polymer Physics, ETH Zürich, Wolfgang-Pauli-Strasse 10, CH-8093 Zürich, Switzerland*
(Received 24 September 2004; published 22 March 2005)

Extensive molecular simulations on a model ferrofluid are performed in order to study magnetoviscous and viscoelastic phenomena in semidilute ferrofluids. Simulation results of the nonequilibrium magnetization, shear viscosity, and normal stress differences are presented. Rotational and configurational contributions to the shear viscosity are analyzed and their influence on the magnetoviscous effect is discussed. The simplified model of noninteracting magnetic dipoles describes the nonequilibrium magnetization and the rotational viscosity, but does not account for configurational viscosity contributions and normal stress differences. Improved mean-field models that overcome these limitations show good agreement with the simulation results for weak dipolar interactions where the models should apply. Comparisons to simulation results for various interaction strengths allow us to determine the range of validity of the mean-field models.

DOI: 10.1103/PhysRevE.71.031205 PACS number(s): 47.65.+a, 75.50.Mm, 47.32.−y, 83.80.Hj

I. INTRODUCTION

The manipulation of viscous properties of fluids by magnetic fields (magnetoviscous effect) has attracted considerable interest both for technical and medical applications as well as from a theoretical point of view [1–3]. While the dynamical properties of highly diluted ferrofluids are well described by the kinetic model of noninteracting (NI) ferromagnetic particles [4], experimental observations on various ferrofluids demonstrate a quantitative and qualitative different behavior (see, e.g., [5] and Odenbach and Thurm in [1] as well as references therein). In this work, we present molecular simulation results on magnetoviscous and viscoelastic effects in a model ferrofluid for different concentrations and dipolar interaction strengths. Results on the formation of nonequilibrium structures and their relation to dynamical properties help to improve the understanding of the magnetoviscous effect from a microscopic point of view. The present study is also helpful to test several assumptions underlying improved kinetic models [6–9], in particular the dynamical mean-field (DMF) theory developed in Ref. [9] and to provide a microscopic basis for thermodynamic theories [10]. Contrary to previous Brownian or Stokesian dynamics simulations [11–13], we focus here on semidilute ferrofluids with weak dipolar interactions. This regime is of direct relevance for various commercial ferrofluids [2]. On the other hand, simulation results in this regime can be compared to the predictions of the model of noninteracting dipoles and dynamical mean-field theory for weakly interacting ferrofluids. These comparisons help to clarify the role of weak dipolar interactions for dynamical properties. In [14], simulation studies similar to the ones presented here have been performed, but only for small system sizes and in two dimensions only.

The paper is organized as follows. In Sec. II, the model system is formulated. The equations of motion are given explicitly as well as the relevant macroscopic quantities. Dimensionless quantities are introduced and the numerical implementation is described. The simplified NI and DMF reference models are reviewed in Sec. III. Simulation results are reported and compared against NI and DMF models, as well as empirical knowledge, in Sec. IV. Conclusions are offered in Sec. V.

II. MODEL FORMULATION

We consider a system of N identical spherical particles of diameter σ at particle number density $n=N/V$. Each particle carries an embedded magnetic point dipole moment of strength m. The position and magnetic moment of particle j are denoted by $\boldsymbol{r}_j$ and $\boldsymbol{m}_j=m\boldsymbol{u}_j$, respectively, where the three-dimensional unit vector $\boldsymbol{u}_j$ denotes the orientation of the magnetic moment.

Particles j and k interact with each other by dipole-dipole interactions Φ^{dd} and a spherically symmetric repulsive potential Φ^{s} which describes steric interaction effects,

$$\Phi_{jk}(\boldsymbol{r}_j,\boldsymbol{u}_j,\boldsymbol{r}_k,\boldsymbol{u}_k)=\Phi^{\mathrm{dd}}(\boldsymbol{r}_{jk},\boldsymbol{u}_j,\boldsymbol{u}_k)+\Phi^{\mathrm{s}}(r_{jk}), \tag{1}$$

where $\boldsymbol{r}_{jk}\equiv\boldsymbol{r}_j-\boldsymbol{r}_k$ and $r_{jk}=|\boldsymbol{r}_{jk}|$ is the relative distance between the particles. The dipole-dipole interaction is given by

$$\Phi^{\mathrm{dd}}(\boldsymbol{r},\boldsymbol{u},\boldsymbol{u}')=\frac{m^2}{4\pi\mu_0 r^3}[\boldsymbol{u}\cdot\boldsymbol{u}'-3(\boldsymbol{u}\cdot\hat{\boldsymbol{r}})(\boldsymbol{u}'\cdot\hat{\boldsymbol{r}})], \tag{2}$$

where $\hat{\boldsymbol{r}}=\boldsymbol{r}/r$ and $\mu_0=4\pi\times10^{-7}$ H/m. For a better comparison to the results [15], the potential Φ^{s} is also chosen as a (truncated and shifted) Lennard-Jones potential $\Phi^{\mathrm{s}}(r)=4\epsilon[C(r)-C(r_{\mathrm{cut}})]$, for $r\leqslant r_{\mathrm{cut}}$ and $\Phi^{\mathrm{s}}=0$ for $r>r_{\mathrm{cut}}$, where $C(r)=(\sigma/r)^{12}-(\sigma/r)^6$, r_{cut} is the cut off radius, and $-\epsilon$ is the value of Φ^{s} in the minimum. In particular, we choose the so-called Weeks-Chandler-Anderson (WCA) potential as in [15], i.e., $r_{\mathrm{cut}}=2^{1/6}\sigma$, such that the potential is cut off in the

*Corresponding author. Electronic address: ilg@physik.tu-berlin.de

minimum, resulting in a purely repulsive interaction with continuous derivative at r_{cut}. In addition to the pair interactions, the particles are exposed to a homogeneous magnetic field $\boldsymbol{H}$. Therefore, the magnetic dipole moment of particle j contributes $\Phi_j^H = -m\boldsymbol{u}_j \cdot \boldsymbol{H}$ to the total potential energy $\Phi = \Sigma_j(\Phi_j^H + \Sigma_k \Phi_{jk})$.

A. Translational and orientational dynamics

The solvent of the ferrofluid is not considered explicitly here. Instead, it is assumed that collisions keep the ferromagnetic particles in thermal equilibrium with the solvent. To model this effect, friction and Brownian forces are added to the equations of motion derived from Φ so as to ensure the fluctuation-dissipation theorem [16,17]. If M and $\boldsymbol{\Theta}$ denote the mass and the moment of inertia tensor of the ferromagnetic particles, the equations of motion read [14,15,17]

$$M\dot{\boldsymbol{v}}_j = \sum_{k=1}^{N}{}' \boldsymbol{F}_{jk} - \zeta_t(\boldsymbol{v}_j - \boldsymbol{v}(\boldsymbol{r}_j)) + \sqrt{2k_{\mathrm{B}}T\zeta_t}\,\dot{\boldsymbol{W}}_j^t, \tag{3}$$

$$\boldsymbol{\Theta}\cdot\dot{\boldsymbol{\omega}}_j = m\boldsymbol{u}_j \times \boldsymbol{H} + \sum_{k=1}^{N}{}' \boldsymbol{N}_{jk}^{\mathrm{dd}} - \zeta_{\mathrm{rot}}(\boldsymbol{\omega}_j - \boldsymbol{\Omega}(\boldsymbol{r}_j)) + \sqrt{2k_{\mathrm{B}}T\zeta_{\mathrm{rot}}}\,\dot{\boldsymbol{W}}_j^{\mathrm{rot}}, \tag{4}$$

where $\boldsymbol{v}_j = \dot{\boldsymbol{r}}_j$ and $\boldsymbol{\omega}_j = \boldsymbol{u}_j \times \dot{\boldsymbol{u}}_j$ denote the translational and angular velocities of particle j, respectively. The forces $\boldsymbol{F}_{jk}$ and torques $\boldsymbol{N}_{jk}^{\mathrm{dd}}$ are obtained from the interaction potential by

$$\boldsymbol{F}_{jk} = -\partial\Phi_{jk}/\partial\boldsymbol{r}_{jk}, \quad \boldsymbol{N}_{jk}^{\mathrm{dd}} = -\boldsymbol{\mathcal{L}}_j\Phi_{jk} \tag{5}$$

(no summation convention), where $\boldsymbol{\mathcal{L}}_j \equiv \boldsymbol{u}_j \times \partial/\partial\boldsymbol{u}_j$ is the rotational operator. The first term on the right hand side of Eq. (4) equals $-\boldsymbol{\mathcal{L}}_j\Phi_j^H$, which is the torque exerted by the magnetic field. Primes on summation symbols imply that the term $j=k$ should be omitted from the sums. Boltzmann's constant and the absolute temperature are denoted by k_{B} and T, while ζ_t and ζ_{rot} are the translational and rotational friction coefficients, respectively. For a sphere of diameter σ in a solvent with viscosity η_{s}, these coefficients are given by $\zeta_t = 3\pi\eta_{\mathrm{s}}\sigma$ and $\zeta_{\mathrm{rot}} = \pi\eta_{\mathrm{s}}\sigma^3$. Frequent collisions of the ferromagnetic particles with the solvent molecules are assumed on short time scales. Accordingly, the effect of the collisions is modeled by $2N$ independent, three-dimensional Wiener processes $\boldsymbol{W}_j^x(t)$ with $\langle \boldsymbol{W}_j^x(t)\rangle = \boldsymbol{0}$ and $\langle \boldsymbol{W}_j^x(t)\boldsymbol{W}_k^x(t')\rangle = \min(t,t')\delta_{jk}\boldsymbol{1}$ for $x = t$, rot. Averages over different realization of the Wiener processes are denoted by $\langle\cdot\rangle$. Equations (3) and (4) account for the hydrodynamic drag in the presence of a flow field $\boldsymbol{v}(\boldsymbol{r})$ with the local vorticity $\boldsymbol{\Omega}(\boldsymbol{r}) \equiv \frac{1}{2}\boldsymbol{\nabla}\times\boldsymbol{v}(\boldsymbol{r})$. Hydrodynamic interactions are not included in Eqs. (3) and (4), which therefore correspond to the so-called "free draining" limit. In our simulations we obtain particle trajectories and orientations from Eqs. (3) and (4) which essentially involve, in addition to the number N and number density n of particles, the macroscopic flow field $\boldsymbol{v}(\boldsymbol{r})$, solvent viscosity η_{s}, dipole moment strength m, mass M, and moment of inertia tensor $\boldsymbol{\Theta}$ of the particles, temperature T, and magnetic field $\boldsymbol{H}$ as free parameters. See Sec. II C for a dimensionless version of these dynamical equations.

B. Macroscopic quantities, viscosity coefficients

The viscous and viscoelastic behavior of the model system is described by the viscous pressure tensor $\boldsymbol{P}$, governing the momentum balance equation $\rho\dot{\boldsymbol{v}} = -\boldsymbol{\nabla}\cdot\boldsymbol{P} + \boldsymbol{f}_{\mathrm{M}}$, where $\boldsymbol{f}_{\mathrm{M}}$ is the magnetic force density. For the spatially homogeneous system to be considered in the remainder of this article, the viscous pressure tensor $\boldsymbol{P}$ is defined by [17]

$$\boldsymbol{P} = p_0\boldsymbol{1} - \eta_{\mathrm{s}}\boldsymbol{D} + \frac{1}{2V}\sum_{j,k}{}' \boldsymbol{r}_{jk}\boldsymbol{F}_{jk} + 3\eta_{\mathrm{s}}\phi\,\boldsymbol{\epsilon}\cdot(\overline{\boldsymbol{\omega}} - \boldsymbol{\Omega}). \tag{6}$$

The viscous stress tensor $\boldsymbol{T}$ is defined as the negative viscous pressure tensor, $\boldsymbol{T} = -\boldsymbol{P}$. The first term on the right hand side of Eq. (6) represents the isotropic pressure. The second term is the contribution of the Newtonian solvent with viscosity η_{s} and the symmetric velocity gradient $\boldsymbol{D} \equiv \frac{1}{2}[\boldsymbol{\nabla}\boldsymbol{v} + (\boldsymbol{\nabla}\boldsymbol{v})^T]$. The contribution of the internal forces is described by the third term. The last term describes rotational friction if the average angular velocity of the particles $\overline{\boldsymbol{\omega}} = (1/N)\Sigma_{i=1}^N\boldsymbol{\omega}_i$ differs from the local vorticity of the flow $\boldsymbol{\Omega}$ (see, e.g., Shliomis in [1]). In Eq. (6), we have introduced the hydrodynamic volume (or packing) fraction $\phi = n\pi\sigma^3/6$. The total antisymmetric tensor of rank 3 (Levi-Civita) is denoted by $\boldsymbol{\epsilon}$, i.e., $\boldsymbol{\epsilon}:(\boldsymbol{ab}) = \boldsymbol{a}\times\boldsymbol{b}$ for the dyadic $\boldsymbol{ab}$ constructed by arbitrary vectors $\boldsymbol{a}$ and $\boldsymbol{b}$. Like any second rank tensor, the viscous pressure tensor $\boldsymbol{P}$ can be decomposed uniquely into its isotropic, symmetric traceless and antisymmetric part [3],

$$\boldsymbol{P} = p\boldsymbol{1} + \overline{\boldsymbol{P}} + \frac{1}{2}\boldsymbol{\epsilon}\cdot\boldsymbol{p}^{\mathrm{a}}. \tag{7}$$

The symbol $\overline{\cdots}$ denotes the symmetric traceless part of a tensor. The antisymmetric part involves the pseudovector $\boldsymbol{p}^{\mathrm{a}} = -\boldsymbol{\epsilon}:\boldsymbol{P}$. Taking the symmetric traceless part of Eq. (6) we obtain

$$\overline{\boldsymbol{P}} = -\eta_{\mathrm{s}}\boldsymbol{D} + \frac{1}{2V}\sum_{j,k}{}' \overline{\boldsymbol{r}_{jk}\boldsymbol{F}_{jk}}. \tag{8}$$

Inserting the equation of motion (4) into (6) and averaging over the particles, the antisymmetric part of the viscous pressure tensor is given by

$$\boldsymbol{p}^{\mathrm{a}} = \boldsymbol{M}\times\boldsymbol{H} \tag{9}$$

where $\boldsymbol{M} = M_{\mathrm{sat}}\overline{\boldsymbol{u}}$ denotes the macroscopic magnetization resulting from the magnetic moments $\boldsymbol{m}_j = m\boldsymbol{u}_j$, $\overline{\boldsymbol{u}} = (1/N)\Sigma_i\boldsymbol{u}_i$ is the average orientation of the particles, and $M_{\mathrm{sat}} = nm$ is the saturation magnetization. Thus, the viscous pressure tensor $\boldsymbol{P}$ is symmetric in the absence of a magnetic field. In the presence of a local magnetic field, an antisymmetric contribution to the viscous pressure arises due to the torques exerted by the magnetic field on the particles. This torque maintains the difference of average particle rotation and local vorticity of the flow, $\overline{\boldsymbol{\omega}} - \boldsymbol{\Omega}$. We mention that the total pressure tensor, i.e., the sum of the viscous and Maxwell pressure tensors, is symmetric due to conservation of total angular momentum. Note that the ensemble average is denoted by an overbar, while averages over the thermal noise are indicated by angu-

lar brackets. Since we consider independent Wiener processes, it follows that for large systems $\langle \boldsymbol{W}_j(t)\rangle = \overline{\boldsymbol{W}_j(t)} = \boldsymbol{0}$.

In a steady shear flow with shear rate $\dot\gamma$ and the linear velocity profile $\boldsymbol{v}=(\dot\gamma y,0,0)$, several viscometric functions can be defined. The (total) shear viscosity η_{yx} is defined as $\eta_{yx}=-P_{yx}/\dot\gamma$. An important role in the theory of ferrofluid dynamics plays the so-called rotational viscosity $\eta_{\rm rot}$ which is the shear viscosity resulting from the antisymmetric part of the pressure tensor only, $\eta_{\rm rot}=-p_z^{\rm a}/(2\dot\gamma)$. In nonpolar complex fluids such as polymers, the shear viscosity is dominated by the configurational viscosity, defined by $\eta_{yx}^{\rm conf}=-P_{yx}^{\rm conf}/\dot\gamma$, where the configurational contribution to the stress tensor $\boldsymbol{P}^{\rm conf}$ is given by the second term on the right hand side of Eq. (8). Furthermore, the first and second normal stress differences are defined by $N_1=P_{yy}-P_{xx}$ and $N_2=P_{zz}-P_{yy}$, respectively [18]. Experimental results on the magnetoviscosity are frequently displayed using the relative viscosity increase $\Delta\eta/\eta_0$, where $\Delta\eta=\eta_{yx}-\eta_0$ and η_0 is the viscosity in the absence of a magnetic field.

C. Dimensionless equations

For further analytical studies as well as the numerical implementation of the equations, it is convenient to use dimensionless quantities. The dimensionless length and time are given by $r^*=r/\sigma$ and $t^*=t/\tau_0$, $\tau_0=(M\sigma^2/\epsilon)^{1/2}$, respectively. Similarly, the reduced temperature is defined by $T^*=k_{\rm B}T/\epsilon$, reduced dipolar moment by $m^*=m(4\pi\mu_0\epsilon\sigma^3)^{-1/2}$, magnetic field $\boldsymbol{H}^*=\boldsymbol{H}(4\pi\mu_0\sigma^3/\epsilon)^{1/2}$, and moment of inertia $\boldsymbol{\Theta}^*=\boldsymbol{\Theta}/M\sigma^2$. The dimensionless friction coefficients are given by $\zeta_{\rm t}^*=\zeta_{\rm t}(\sigma^2/M\epsilon)^{1/2}$ and $\zeta_{\rm rot}^*=\zeta_{\rm rot}(M\sigma^2\epsilon)^{-1/2}$. The dipolar interaction parameter λ,

$$\lambda \equiv \frac{m^2}{4\pi\mu_0 k_{\rm B}T\sigma^3} = \frac{m^{*2}}{T^*}, \tag{10}$$

is a measure for the strength of the dipolar interactions compared to the thermal energy. The Langevin parameter h,

$$h \equiv \frac{mH}{k_{\rm B}T} = \frac{m^*H^*}{T^*}, \tag{11}$$

is the energy of a magnetic dipole in the magnetic field relative to the thermal energy. Using these quantities, the dimensionless equations of motion for the N particles read

$$\dot{\boldsymbol{v}}_j^* = {\sum_{k=1}^{N}}' \boldsymbol{F}_{jk}^* - \zeta_{\rm t}^*(\boldsymbol{v}_j^* - \boldsymbol{v}^*(\boldsymbol{r}_j^*)) + \sqrt{2T^*\zeta_{\rm t}^*}\,\dot{\boldsymbol{W}}_j^*, \tag{12}$$

$$\boldsymbol{\Theta}^*\cdot\dot{\boldsymbol{\omega}}_j^* = T^*\boldsymbol{u}_j\times\boldsymbol{h} + {\sum_{k=1}^{N}}' \boldsymbol{N}_{jk}^{\rm dd*} - \zeta_{\rm rot}^*(\boldsymbol{\omega}_j^* - \boldsymbol{\Omega}^*(\boldsymbol{r}_j^*)) + \sqrt{2T^*\zeta_{\rm rot}^*}\,\dot{\boldsymbol{W}}_j^*. \tag{13}$$

In Eqs. (12) and (13), the dimensionless forces and torques have been defined by $\boldsymbol{F}_{jk}^*=(\tau_0^2/M\sigma^2)\boldsymbol{F}_{jk}$ and $\boldsymbol{N}_{jk}^{\rm dd*}=(\tau_0^2/M\sigma^2)\boldsymbol{N}_{jk}^{\rm dd}$, respectively. Both of them are proportional to the dipolar interaction parameter λ. The dimensionless pressure tensor is defined by $\boldsymbol{P}^*=(\sigma^3/\epsilon)\boldsymbol{P}$. Besides N and ϕ, the dimensionless parameters governing the dynamics (12) and (13) are $h,\lambda,\zeta_{\rm t}^*$, and T^*.

III. SIMPLIFIED MODELS FOR WEAK DIPOLAR INTERACTION

The time evolution equations (3) and (4) or (12) and (13) cannot be solved analytically except for special cases. In order to better understand the dynamical behavior described by these equations, it is useful to consider simplified models that allow further analytical investigations. In particular, a dynamical mean-field model has been proposed recently by two of the authors [9] that extends the existing model of noninteracting magnetic dipoles [4] to the weakly interacting regime. In order to make the paper self-contained, we briefly review the more general DMF model, and summarize its implications to be checked against simulation results in Sec. IV.

A. Effective local field

If dipolar interactions can be neglected, the orientational dynamics Eq. (4) decouples from the translational motion and the magnetic properties of the system can be studied in terms of the phase space variables $\boldsymbol{u}$ and $\boldsymbol{\omega}$ only. On time scales where the inertia term can also be neglected, $\boldsymbol{\Theta}\cdot\dot{\boldsymbol{\omega}}=0$, Eq. (4) reduces to the Langevin formulation of the kinetic NI model [4,19]

$$\boldsymbol{\omega} = \boldsymbol{\Omega} - \frac{1}{\zeta_{\rm rot}}\boldsymbol{\mathcal{L}}\Phi + \sqrt{\frac{2k_{\rm B}T}{\zeta_{\rm rot}}}\,\dot{\boldsymbol{W}}, \tag{14}$$

with $\boldsymbol{\mathcal{L}},\boldsymbol{\Omega}$, and $\boldsymbol{W}$ defined in Sec. II A. The potential Φ is identified with the magnetic field contribution Φ^H; thus presently $\boldsymbol{\mathcal{L}}\Phi=-m\boldsymbol{u}\times\boldsymbol{H}$. The corresponding Fokker-Planck Smoluchowski equation for the orientational distribution function $f(\boldsymbol{u};t)$ is given by [4]

$$\frac{\partial f}{\partial t} = -\boldsymbol{\mathcal{L}}\cdot\left[\left(\boldsymbol{\Omega} - \frac{1}{\zeta_{\rm rot}}\boldsymbol{\mathcal{L}}\Phi\right)f\right] + \frac{k_{\rm B}T}{\zeta_{\rm rot}}\boldsymbol{\mathcal{L}}^2 f. \tag{15}$$

The magnetization is determined from f by $\boldsymbol{M}=M_{\rm sat}\langle\boldsymbol{u}\rangle$, where $\langle\boldsymbol{u}\rangle=\int d^2u\,\boldsymbol{u}f(\boldsymbol{u})$. For low densities, the effect of weak dipolar interactions on the equilibrium magnetization can be described to leading order by an effective local magnetic field $\boldsymbol{H}_{\rm loc}=\boldsymbol{H}+\frac{1}{3}\boldsymbol{M}$, or in dimensionless form $\boldsymbol{h}_{\rm loc}=\boldsymbol{h}+\chi_L\langle\boldsymbol{u}\rangle$ [20,21]. In these theories, the leading order contribution of dipolar interactions appears in the form of the Langevin susceptibility $\chi_L=8\lambda\phi$, where λ is given by Eq. (10) and ϕ denotes the hydrodynamic volume fraction introduced above. While higher order terms in λ and ϕ have been considered for the equilibrium magnetic properties (see [20,21] and references therein), here only the lowest order contribution is taken into account for the dynamical properties. Including these higher order terms into the dynamics is left for further studies. The energy of a magnetic dipole in the local field $\boldsymbol{H}_{\rm loc}$ is given by

$$\Phi_{\rm loc} = -m\boldsymbol{u}\cdot\boldsymbol{H}_{\rm loc}. \tag{16}$$

The mean-field character of the potential (16) is evident. In a constant magnetic field $\boldsymbol{H}$ with strength H, the equilibrium

magnetization is found from Eq. (16) to be given by $M/M_{\mathrm{sat}}=S_1(h)=L_1(h_{\mathrm{loc}})$. The saturation magnetization is defined by $M_{\mathrm{sat}}=nm$ and $L_1(x)=\coth(x)-1/x$ denotes the Langevin function. Dipolar interactions therefore lead to an enhanced magnetization which to leading order in λ is given by $S_1(h)=L_1(h)+\chi_L L_1'(h)L_1(h)$, where the prime denotes a total derivative. Recent simulation studies have shown that the magnetization of weakly interacting ferrofluids is indeed well described in terms of this local field [15].

B. Dynamical mean field

Following similar strategies widely used in the dynamics of nematic liquid crystals [18,22,23], we assume that Eq. (16) represents a meaningful potential also for dynamical properties. In a given external flow field $\boldsymbol{v}(\boldsymbol{r})$, additional contributions from dipolar interactions appear due to the disturbance of the equilibrium structure. The mean dipolar interaction energy can be calculated self-consistently from the orientational distribution function f,

$$\Phi_{\mathrm{SCF}}(\boldsymbol{u};f)=\frac{n}{k_{\mathrm{B}}T}\int d^2u'\int d^3r\,\Phi^{\mathrm{dd}}(\boldsymbol{r},\boldsymbol{u},\boldsymbol{u}')g(\boldsymbol{r},\boldsymbol{u},\boldsymbol{u}')f(\boldsymbol{u}') \tag{17}$$

where g denotes the pair correlation function [9]. For weak dipolar interactions, $g(\boldsymbol{r},\boldsymbol{u},\boldsymbol{u}')\approx g(\boldsymbol{r})$ becomes the pair correlation function of the reference fluid without dipolar interactions. Note that in equilibrium the leading order term linear in λ of Eq. (17) vanishes by symmetry, since in this case $g_{\mathrm{eq}}(\boldsymbol{r})=g_{\mathrm{eq}}(r)$ is radially symmetric and the angular average of Φ^{dd} over distance vectors $\boldsymbol{r}$ vanishes.

In an external flow field, the equilibrium structure is disturbed leading to an anisotropic pair correlation function [24]. In order to estimate the flow-induced distortion of the pair correlation function, we follow the proposition of one of the authors in [25] and assume affine deformation with the flow accompanied by an exponential relaxation toward the equilibrium state,

$$\frac{\partial g}{\partial t}+\boldsymbol{r}\cdot(\boldsymbol{\nabla v})\cdot\boldsymbol{\nabla}g=-\frac{1}{\tau}(g-g_{\mathrm{eq}}). \tag{18}$$

On time scales long compared to the structural relaxation time τ, Eq. (18) predicts a nonequilibrium stationary structure which to lowest order in the velocity gradients is described by

$$g(\boldsymbol{r})=g_{\mathrm{eq}}(r)-\tau\boldsymbol{D}:\hat{\boldsymbol{r}}\hat{\boldsymbol{r}}rg_{\mathrm{eq}}'(r), \tag{19}$$

where $\boldsymbol{D}$ has been defined after Eq. (6). Results of recent nonequilibrium molecular dynamics simulations of a dipolar model fluid [26] are in good agreement with Eq. (19). Inserting Eq. (19) into Eq. (17) and combining with the local field (16), the effective potential of the magnetic field and dipolar interactions is given by

$$\frac{\Phi_{\mathrm{eff}}}{k_{\mathrm{B}}T}\equiv\frac{\Phi_{\mathrm{loc}}+\Phi_{\mathrm{SCF}}}{k_{\mathrm{B}}T}=-\boldsymbol{u}\cdot\boldsymbol{h}_{\mathrm{loc}}+\frac{6}{5}\chi_{\mathrm{L}}\tau\boldsymbol{u}\cdot\boldsymbol{D}\cdot\langle\boldsymbol{u}\rangle. \tag{20}$$

Inserting the effective potential Eq. (20) into the kinetic equation (15) defines the dynamical mean-field model of weakly interacting magnetic dipoles proposed in [9]. In the limit $\chi_{\mathrm{L}}\to 0$, the kinetic model of noninteracting magnetic dipoles is recovered as a special case.

Neither the NI nor the DMF model leads to closed form expressions for the magnetization and viscosity. In the following, to overcome these difficulties, both models are treated within the effective field approximation, proposed in [4]. Previous studies [7,19] have shown that the effective field approximation gives very accurate results for the NI model as well as generalizations thereof. Therefore, we employ the effective field approximation also in the DMF model.

C. Implication for the pressure tensor

Within the kinetic models, the magnetization dynamics is obtained from Eq. (15). The nonequilibrium magnetization in turn determines the antisymmetric pressure (9) and therefore the rotational viscosity. In order to calculate the symmetric traceless part of the pressure tensor (8), we take advantage of the fact that for homogeneous systems this contribution can be reexpressed in terms of the pair correlation function. Using Eq. (20) for the effective potential and the analog of Eq. (19) for the pair correlation function for weak dipolar interactions, the viscous pressure tensor becomes [9]

$$\boldsymbol{P}=p\mathbf{1}-2\tilde{\eta}_0\boldsymbol{D}-7a\overline{\langle\boldsymbol{u}\rangle\langle\boldsymbol{u}\rangle\times\boldsymbol{\Omega}}-2a(c_1-3)\overline{\boldsymbol{D}\cdot\langle\boldsymbol{u}\rangle\langle\boldsymbol{u}\rangle}+\frac{1}{2}nk_{\mathrm{B}}T(\langle\boldsymbol{u}\rangle\boldsymbol{h}-\boldsymbol{h}\langle\boldsymbol{u}\rangle). \tag{21}$$

In Eq. (21), we have introduced $a\equiv 2\eta_{\mathrm{s}}\kappa\lambda\phi^2$, where $\kappa\equiv 72\tau/(35\tau_{\mathrm{rot}})$ and $\tau_{\mathrm{rot}}=\pi\eta_{\mathrm{s}}\sigma^3/(2k_{\mathrm{B}}T)$ denotes the rotational diffusion time of a sphere with diameter σ in a solvent with viscosity η_{s}. The shear viscosity of the isotropic suspension is $\eta_0=\eta_{\mathrm{s}}(1+\frac{5}{2}\phi+b\phi^2)$, where $b\equiv\frac{7}{6}c_4\kappa$ and $\tilde{\eta}_0\equiv\eta_0-\frac{1}{3}(c_1-3)a\langle\boldsymbol{u}\rangle^2$. The coefficients c_k depend on the detailed form of the short range interaction potential. For the WCA potential considered in Sec. II and in the limit of small concentrations where the pair correlation function of the reference fluid can be approximated by $g(r)\approx\exp[-\beta\Phi^{\mathrm{s}}(r)]$ for $r>\sigma$ and zero else, these coefficients take the values $c_1\approx 7.72$ and $c_4\approx 8.36$. A reduced temperature of $T^*=1$ has been assumed. For potentials with softer repulsion higher values of c_1 and c_4 are obtained.

In the absence of dipolar interactions, the pressure tensor is purely antisymmetric if solvent contributions and the isotropic pressure are disregarded. Including dipolar interactions within the mean-field model, we notice from Eq. (21) that the pressure tensor and therefore the viscosity depend not only on the vorticity of the flow but also on the symmetric part of the velocity gradient $\boldsymbol{D}$. Similarly, the nonequilibrium magnetization depends, via the effective potential (20), also on $\boldsymbol{D}$. Such a dependence has nicely been demonstrated in recent experiments on commercial ferrofluids [5].

The only parameter in the DMF model that is not specified so far is the translational relaxation time τ entering the dimensionless quantity κ. In principle, τ can be determined from molecular simulations of structural relaxation in nonmagnetic systems. Here, we use as a rough estimate the time

to travel a particle diameter $\tau \approx \tau_0 = (M\sigma^2/\epsilon)^{1/2}$. With this choice no adjustable parameters are left in the DMF model.

D. Prediction for steady shear flow

A steady shear flow with shear rate $\dot{\gamma}$ and the linear velocity profile $\boldsymbol{v}(\boldsymbol{r}) = (\dot{\gamma}y, 0, 0)$ induces a nonequilibrium magnetization component perpendicular to the magnetic field direction. Here and in the following, we consider the special case where the magnetic field is oriented in the gradient direction of the flow. In the absence of dipolar interactions and for small shear rates, the off-equilibrium magnetization component is to a very good approximation given by $\langle u_x \rangle = \frac{1}{2}\dot{\gamma}\tau_0^{\perp}(h)L_1(h)$, where $\tau_0^{\perp}(h) = 2\tau_{\rm rot}L_1(h)/[h - L_1(h)]$ is the transversal relaxation time [4,19]. Within the dynamic mean-field model, $\langle u_x \rangle$ is given by $\langle u_x \rangle = \frac{1}{2}\dot{\gamma}\tau^{\perp}(h)S_1(h)$, where

$$\tau^{\perp}(h) = \tau_0^{\perp}(h_{\rm loc})[1 + \chi_{\rm L} t_0^{\perp}(h_{\rm loc})] \tag{22}$$

with $t_0^{\perp}(x) = \kappa_0(1 - L_1(x)/x)$, $\kappa_0 = (7/24)\kappa$. To lowest order in dipolar interactions, Eq. (22) reduces to $\tau^{\perp}(h) = \tau_0^{\perp}(h)\{1 + \chi_{\rm L}[t_0^{\perp}(h) + t_1^{\perp}(h)]\}$, with $t_1^{\perp}(x) = L_1'(x) - L_1(x)[L_1^2(x) - L_2(x)]/[x - L_1(x)]$. For details of the derivation we refer the reader to [9].

For the special case of plane Couette flow with the magnetic field oriented in the gradient direction, the shear viscosity calculated from Eq. (21) is given by

$$\eta_{yx} = \eta_0 + \frac{3}{2}\eta_{\rm s}\phi\left(\frac{\tau^{\perp}(h)}{2\tau_{\rm rot}}hS_1(h) + d_y\kappa\chi_{\rm L}S_1^2(h)\right), \tag{23}$$

with $d_y = (c_1/6 - 9/4)/6 \approx -0.16$ for the present case. For vanishing dipolar interactions, Eq. (23) reduces to the result for the rotational viscosity given in [4]. We note that the shear viscosity η_{yx} is modified compared to the NI model not only by replacing the magnetic field with the local mean field in the rotational viscosity, but also due to extra contributions from dipolar and steric interactions. Note also that the contributions of repulsive steric interactions and the attractive part of the dipolar interactions cancel partially. Depending on the detailed form of the steric interaction and the resulting pair correlation function, the coefficient d_y may have either sign. For the special case where $d_y = 0$, Eq. (23) reduces to the expression for the rotational viscosity of the NI model with the magnetic field replaced by the effective local field. In the present case, due to $d_y < 0$, it might happen that the viscosity increase with increasing magnetic field is weaker than in the noninteracting case. From Eq. (21), the normal stress differences are calculated as

$$N_i = 14\psi_i\eta_{\rm s}\kappa\lambda\phi^2\dot{\gamma}\langle u_x\rangle\langle u_y\rangle \tag{24}$$

for $i = 1, 2$, with $\psi_1 = 1$ and $\psi_2 = -(c_1 + \frac{1}{2})/7$. It is evident from Eq. (24) that normal stress differences arise due to dipolar interactions and are therefore absent in the NI model. For low shear rates, $\langle u_y \rangle$ can be replaced by its equilibrium value $S_1(h)$ and $\langle u_x \rangle$ has been obtained above as $\langle u_x \rangle = \frac{1}{2}\dot{\gamma}\tau^{\perp}(h)S_1(h)$. Therefore, N_i simplifies for low rates to $N_i = 7\psi_i\eta_{\rm s}\kappa\lambda\phi^2\dot{\gamma}^2\tau^{\perp}(h)S_1^2(h)$. From this expression we find that $N_1 > 0$ and $N_2 < 0$, which is the case frequently encountered in the rheology of complex fluids [18]. An interesting observation from Eq. (24) is that the ratio $-N_2/N_1 = (c_1 + \frac{1}{2})/7$ is a constant, $-N_2/N_1 \approx 1.17$ in the present case of the WCA potential, independent of the magnetic field, the shear rate, and the dipolar interaction strength. This ratio is determined by the details of the short range interactions and should depend only weakly via c_1 on the volume fraction.

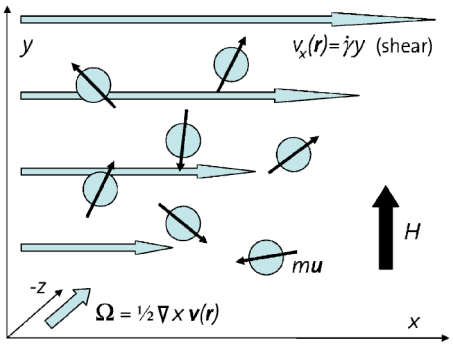

FIG. 1. Schematic plot of the flow geometry together with the orientation of the magnetic field considered in the present study.

Finally, we note that Eq. (24) implies that the ratio of normal stress differences is bounded by $|N_2/N_1| \geqslant 1/14$ due to the property $c_1 \geqslant 0$.

IV. SIMULATION AND RESULTS

Steady shear flows with shear rate $\dot{\gamma}$ and the linear velocity profile $\boldsymbol{v}(\boldsymbol{r}) = (\dot{\gamma}y, 0, 0)$ together with static magnetic fields oriented in the gradient direction of the flow $\boldsymbol{H} = (0, H, 0)$ are considered exclusively in this section. Equilibrium simulations are covered at vanishing shear rate. Figure 1 schematically illustrates the chosen flow geometry together with the magnetic field direction.

In order to study bulk properties in a finite, sheared system, Lees-Edwards periodic boundary conditions [17] are employed. The long range dipolar interactions are handled using the reaction field method [17]. In this method, interactions of particles within a spherical cavity of radius $r_{\rm RF}$ are treated explicitly, while the effect of particles with distances greater than $r_{\rm RF}$ is estimated based on a continuum description. It is assumed that on particle j the effect of particles with distances $r_{ij} > r_{\rm RF}$ can be described by a dielectric continuum which gives rise to a reaction field inside the cavity. The strength of the reaction field is estimated by the magnetization within the cavity, $\boldsymbol{H}_j^{\rm RF} = \tilde{\varepsilon}_{\rm s}\Sigma_i f(r_{ij})\boldsymbol{m}_i$, $f(r) = 0$ for $r > r_{\rm RF}$, with effective dielectric constant $\tilde{\varepsilon}_{\rm s} = 2(\varepsilon_{\rm s} - 1)/(2\varepsilon_{\rm s} + 1)$. The function $f(r)$ can be chosen as a step function $f(r) = 1 - \theta(r - r_{\rm RF})$ with $\theta(x)$ the Heaviside function. In order to avoid problems due to the discontinuity of f at $r_{\rm RF}$, we use a cubic spline interpolation for $0.95 \leqslant r/r_{\rm RF} \leqslant 1$ [17]. Note that the term $i = j$ is included in the sum. We emphasize that the radius of the cavity $r_{\rm RF}$ is always much larger than the cut off radius $r_{\rm cut}$ of the spherical potential $\Phi^{\rm s}$. The validity of the reaction field method in the present context is shown in Sec. IV B.

A. Simulation parameters

The equations of motion (12) and (13) are integrated numerically with a leapfrog algorithm [17]. An adaptive time

step of order $\Delta t^* = 0.001$ is employed in all simulations. The reduced temperature is chosen as $T^* = 1$. The magnetic particles are treated as rigid spheres, where the reduced moment of inertia takes the form $\mathbf{\Theta}^* = \Theta^* \mathbf{1}$ with $\Theta^* = 0.1$. With the help of the rotational diffusion time, the dimensionless friction coefficients can be written as $\zeta^*_{\mathrm{rot}} = 2T^* \tau_{\mathrm{rot}} / \tau_0$ and $\zeta^*_{\mathrm{t}} = 3\zeta^*_{\mathrm{rot}}$. In the simulations we use $\zeta^*_{\mathrm{t}} = 10$. Similar to [15], we use metallic boundary conditions with $\varepsilon_s \to \infty$, resulting in $\tilde{\varepsilon}_s = 1$. Typical values for the cavity radii chosen in the simulations are $r_{\mathrm{RF}}/\sigma = 2.5$, 3.0, and 3.5. The reduced shear rate $\dot{\gamma}^* = \tau_0 \dot{\gamma}$ is varied between 10^{-3} and 10. The simulations are started from initial configurations with particle positions on a regular lattice and random dipole orientations. For each run, the system is integrated for at least 10^5 time steps in order to reach a stationary state. Steady state values of rheological and structural quantities are then extracted as time averages from the subsequent simulations, which are carried out for additional 5×10^5 or more time steps.

Typically, systems with $N = 10\,648$ particles are considered. In order to investigate finite size effects, several simulations have been performed with $N = 512$, 1024, 2048, 5325, and 16 384 particles. Different values for the reduced number density $n^* = (N/V)\sigma^3$ have been chosen, corresponding to packing fractions $\phi = n^* \pi / 6$ ranging from 0.02 to 0.16.

The remaining dimensionless simulation parameters appearing in the equations of motion (12) and (13) are the dimensionless friction coefficient ζ^*_{t}, the dipolar interaction strength λ, and the Langevin parameter h defined in Eqs. (10) and (11), respectively.

B. Equilibrium results

In the absence of flow, $\dot{\gamma}^* = 0$, Eqs. (12) and (13) evolve the system toward the equilibrium state with the corresponding canonical distribution function. Figure 2 shows the resulting equilibrium magnetization as a function of the Langevin parameter h for different volume fractions ϕ and dipolar interaction strengths λ. Comparison to the results of [15] using the Ewald summation technique for dipolar interactions shows very good agreement for $\phi = 0.0393$, $\lambda = 4$ and $\phi = 0.0785$, $\lambda = 2$. Also cluster sizes and their size distribution (not shown) are in very good agreement to the results of [15]. For higher volume fractions with significant dipolar interactions, $\phi = 0.157$, $\lambda = 4$ and $\phi = 0.209$, $\lambda = 2$, the present results are still in good agreement with those obtained in [15] for weak and strong magnetic fields, but show discrepancies around $h = 1$. Therefore, we conclude that the reaction field method gives accurate results in the semidilute regime if dipolar interactions are not too strong. Further studies are limited to this regime.

C. Results for plane shear flow

In the presence of a stationary shear flow, a nonequilibrium stationary state is obtained as the stationary solution to Eqs. (12) and (13). We have verified the convergence of our simulation results with respect to N, the number of simulated particles; see Fig. 3. Furthermore, several simulations with different values of the reaction field cut-off r_{RF} have been carried out showing only very little influence on the observed quantities.

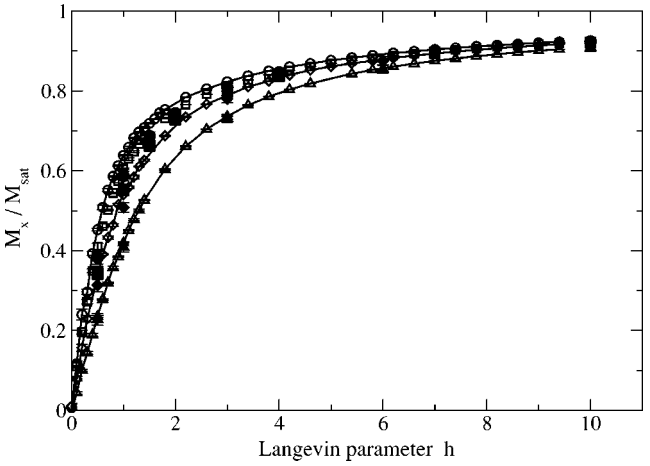

FIG. 2. Normalized equilibrium magnetization as a function of the Langevin parameter h for different volume fractions ϕ and interaction strengths λ. Circles, squares, diamonds, and triangles correspond to $(\phi, \lambda) = (0.157, 4)$, (0.209,2), (0.0393,4), and (0.0785,2), respectively. Big solid symbols are the result of the present simulations using the reaction field method, while small open symbols denote the results employing an Ewald summation technique [15]. Solid lines connecting the data [15] are a guide to the eye.

1. Magnetization

Figure 4 shows the normalized, flow-induced magnetization M_x/M_{sat} as a function of the Langevin parameter h for a shear rate of $\dot{\gamma}^* = 0.1$. Notice that for the present choice of coordinates, M_x denotes the magnetization in the flow direction, perpendicular to the applied magnetic field; see Fig. 1. Results for volume fractions $\phi = 0.05$, 0.1 and different dipo-

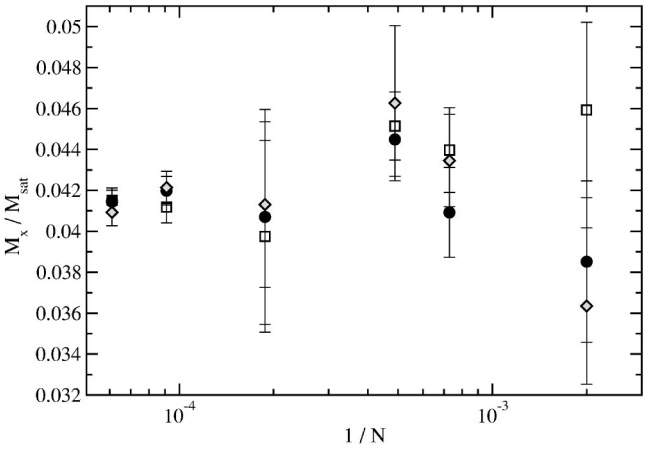

FIG. 3. Nonequilibrium magnetization M_x/M_{sat} as a function of the inverse of the number of particles N. The magnetic field is oriented in the gradient direction of the shear flow; the Langevin parameter is chosen as $h = 1.0$. Squares and diamonds correspond to reaction field cavity radii of $r_{\mathrm{RF}} = 3.0$ and 3.5, respectively, while black circles correspond to $r_{\mathrm{RF}} = 2.5$. The volume fraction and dipolar interaction parameter are chosen as $\phi = 0.05$ and $\lambda = 2.0$, respectively. The reduced shear rate is chosen as $\dot{\gamma}^* = 0.1$.

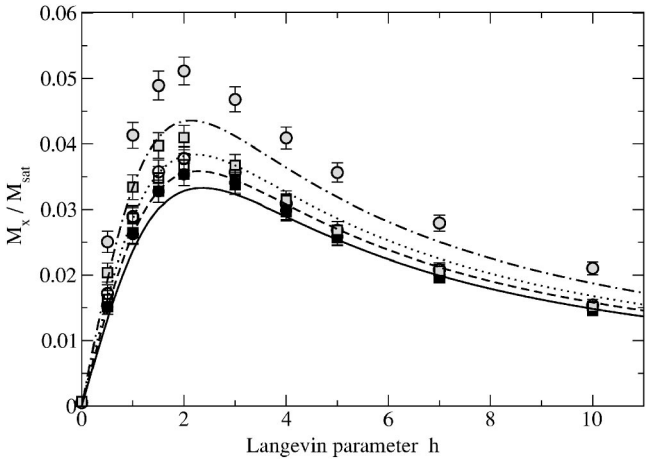

FIG. 4. Nonequilibrium magnetization M_x/M_{sat} as a function of the Langevin parameter h. The magnetic field is oriented in the gradient direction of the shear flow. Circles and squares correspond to volume fractions $\phi=0.05$ and 0.1, respectively. Solid, open, and shaded symbols correspond to different values of λ, resulting in Langevin susceptibilities of $\chi_{\mathrm{L}}=0.2$, 0.4, and 0.8, respectively. The reduced shear rate is chosen as $\dot{\gamma}^*=0.1$. The solid line denotes the result for noninteracting magnetic dipoles, dashed, dotted, and dash-dotted lines correspond to the dynamical mean-field model, for $\chi_{\mathrm{L}}=0.2$, 0.4 and 0.8, respectively. See Sec. III for a summary of both models.

lar interaction strengths $\lambda=0.25$, 0.5, 1.0, 2.0 resulting in Langevin susceptibilities of $\chi_{\mathrm{L}}=0.2$, 0.4, and 0.8 are shown. We observe that dipolar interactions increase the value of M_x/M_{sat} compared to the noninteracting case. This increase is most pronounced around the maximum of M_x/M_{sat} at $h \approx 2$. The DMF model (see Sec. III), describes the behavior of the nonequilibrium magnetization very well for $\chi_{\mathrm{L}}=0.2$ and 0.4. For stronger interactions, $\chi_{\mathrm{L}}=0.8$, however, the increase of M_x compared to the noninteracting case becomes more pronounced. In this range, the DMF model predicts the simulation data semiquantitatively, even though the values of the dipolar interaction parameter $\lambda=1.0$ (for $\phi=0.1$) and 2.0 (for $\phi=0.05$) cannot be considered small and are therefore beyond the range of validity of the DMF model. For this choice of parameters, the nonequilibrium magnetization is no longer a function of χ_{L} only, but depends on ϕ and λ separately. Similar conclusions have been drawn also for the equilibrium magnetization; see Fig. 2 and [15]. Note that the DMF model, like any first order mean-field model, fails to account for such a dependence.

In Fig. 5, the normalized nonequilibrium magnetization perpendicular and parallel to the magnetic field is shown as a function of the reduced shear rate $\dot{\gamma}^*$. The magnetic field is chosen as $h=2$, the volume fraction $\phi=0.05$, and the dipolar interaction parameter $\lambda=0.5$ and 1.0. As predicted by the kinetic models, the nonequilibrium magnetization $\langle u_x \rangle$ increases linearly with $\dot{\gamma}$ for small shear rates, while the magnetization component parallel to the magnetic field decreases monotonically with increasing shear rate. The simulation data are well described by the NI and DMF models (15). The effect of dipolar interactions on the observed quantities is weak for the present choice of parameters and becomes less important for increasing shear rates.

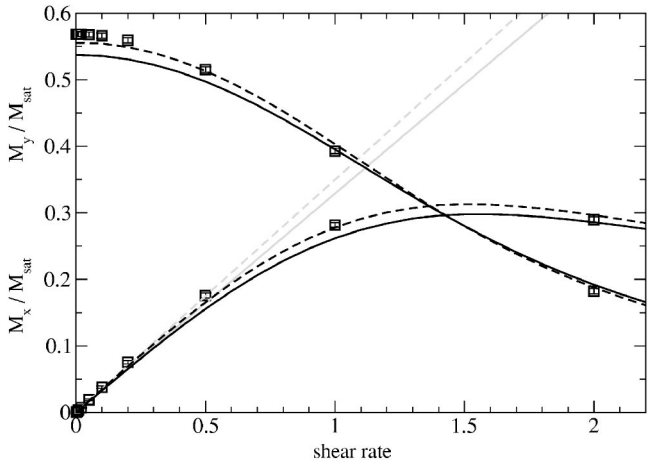

FIG. 5. Nonequilibrium magnetization perpendicular, M_x/M_{sat}, and parallel, M_y/M_{sat}, to the magnetic field as a function of the reduced shear rate $\dot{\gamma}^*$. The magnetic field is oriented in the gradient direction of the shear flow with $h=2$. The volume fraction and dipolar interaction parameter are chosen as $\phi=0.05$ and $\lambda=1.0$, respectively. The solid line denotes the result of the NI model, dashed lines those of the DMF model. Straight gray lines are the result for the low shear rate limit.

2. Rotational viscosity

The rotational viscosity, defined in Sec. II B, is shown in Fig. 6 as a function of the Langevin parameter h for the same conditions and the same parameters as in Fig. 4. Figure 6 illustrates the well-known magnetoviscous effect, i.e., the increase of the shear viscosity with increasing magnetic field strength. Similar to Fig. 4, we observe that dipolar interactions increase the value of the rotational viscosity. For $\chi_{\mathrm{L}}=0.2$, 0.4, the effect of dipolar interactions is weak enough that the NI model describes the simulation data well. For stronger interactions, deviations of the simulation results from the predictions of the NI model become more pronounced. Although the DMF model is not applicable in this

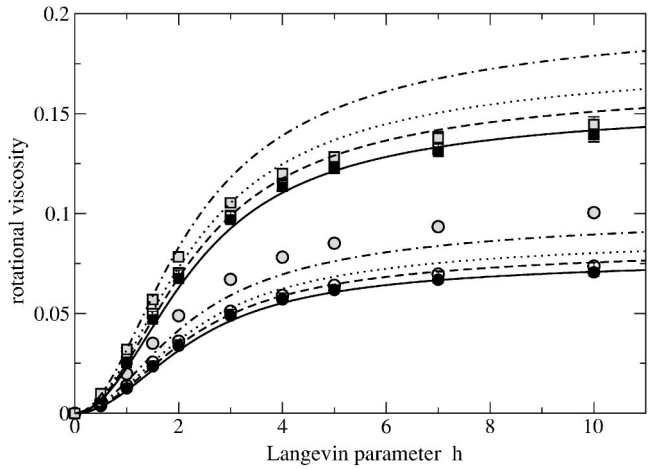

FIG. 6. Reduced rotational viscosity η^*_{rot} as a function of the Langevin parameter h. The same conditions and the same symbols as in Fig. 4 are chosen, in particular, $\dot{\gamma}^*=0.1$. The solid and dashed lines denote results for the NI and DMF models, respectively.

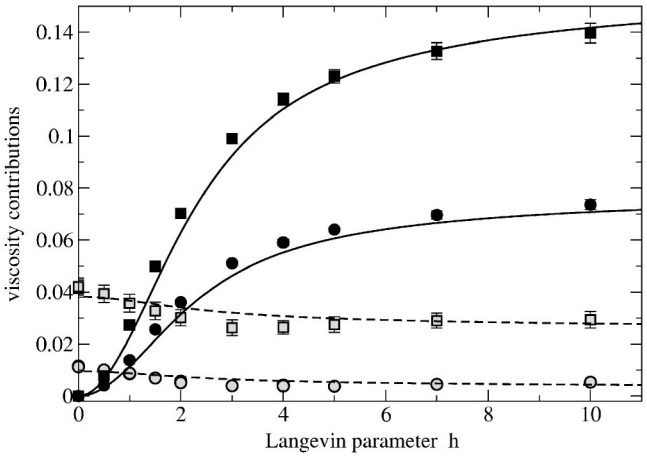

FIG. 7. Different contributions to the reduced shear viscosity η_{yx}^{*} as a function of the Langevin parameter h. Circles and squares correspond to $\phi=0.05$, $\lambda=1.0$ and $\phi=0.1$, $\lambda=0.5$, respectively. Solid and gray symbols show the rotational and configurational contributions, respectively. The solid lines are the predictions of the NI model, dashed lines the additional prediction of the configurational contribution by the DMF model. The same flow conditions as before are used, with a reduced shear rate of $\dot{\gamma}^{*}=0.1$.

case, its predictions are nevertheless included in Fig. 4. While the results for $\phi=0.05$, $\lambda=2.0$ are rather well described by the DMF model, predictions for $\phi=0.1$, $\lambda=1.0$ are much less reliable. Note that the DMF model underpredicts this increase for $\phi=0.05$ and overpredicts for $\phi=0.1$.

3. Contributions to shear viscosity

Not only the rotational but also the configurational contribution defined in Sec. II B are shown in Fig. 7 as a function of the Langevin parameter h. From the figure we notice that the configurational shear viscosity $\eta_{yx}^{\mathrm{conf}}$ (see Sec. II B) is more or less independent of h. Therefore we conclude that although dipolar and spherical interactions contribute to the value of the shear viscosity, the magnetic field dependence is well described by the rotational viscosity only. We note that the DMF model provides an accurate description of the configurational viscosity contribution for the present choice of parameters; see the dashed lines in Fig. 7.

Experimental results on the magnetoviscosity are frequently displayed using the relative viscosity increase $\Delta\eta/\eta_0$, where $\Delta\eta=\eta_{yx}-\eta_0$ and η_0 is the viscosity in the absence of a magnetic field. Figure 8 shows $\Delta\eta/\eta_0$ as a function of the Langevin parameter h. Comparing Fig. 6 to Fig. 8 we note that although increasing dipolar interactions lead to an increase of the shear viscosity η_{yx}, the relative viscosity change $\Delta\eta/\eta_0$ might decrease with increasing dipolar interaction strength due to the increase of η_0; see Fig. 7. At the end of Sec. III, we discussed this possibility on the basis of the DMF model. It is interesting to note that $\Delta\eta/\eta_0$ indeed decreases with increasing λ in the case $\phi=0.1$ for all values of λ investigated. On the other hand, for $\phi=0.05$ and $\lambda=2$, the relative viscosity increase is higher than in the noninteracting case. The predictions of the DMF model show good agreement with the simulation results for $\phi=0.05$.

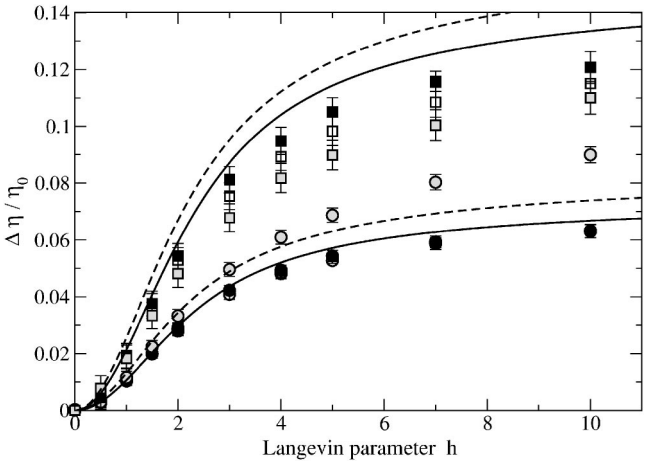

FIG. 8. The relative viscosity change $\Delta\eta/\eta_0-1$ is shown as a function of the Langevin parameter h. The same conditions and the same symbols as in Fig. 4 are used. The solid lines correspond to the NI model, dashed lines to the DMF model ($\phi=0.05$, $\lambda=2.0$ and $\phi=0.1$, $\lambda=1.0$) prediction.

The total viscosity (see Sec. II B) as a function of the volume fraction ϕ (in the absence of a magnetic field and) for a rather strong field $h=20$ is plotted in Fig. 9. The dipolar interaction parameter is chosen as $\lambda=0.5$, 1.0, and 2.0. For low volume fractions $\phi\lesssim 0.05$, the viscosity increases linearly with ϕ, followed by a stronger increase for higher volume fractions. The solid line gives the maximum viscosity increase $\frac{3}{2}\eta_s\phi$ as predicted by the NI model. The simulations show that due to dipolar interactions, the viscosity increase can be significantly larger than predicted by the NI model. This conclusion is in qualitative agreement with experimental results on magnetite based ferrofluids [27]. The DMF model predicts an additional quadratic viscosity increase, both in the absence of a magnetic field and in a strong mag-

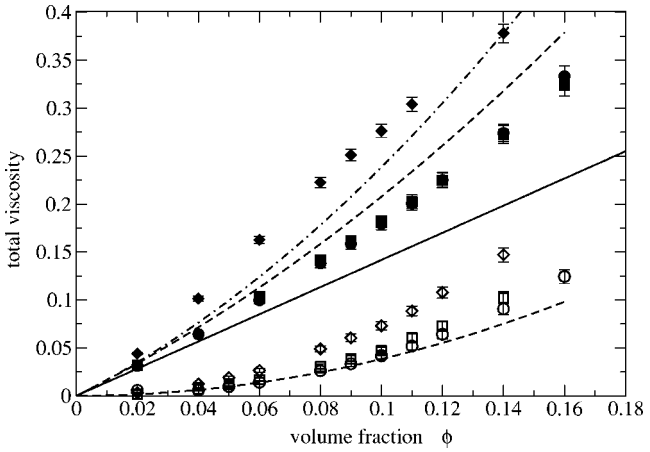

FIG. 9. Reduced shear viscosity η_{yx}^{*} as a function of the volume fraction ϕ. Open symbols correspond to $h=0$, while solid black symbols show the result for $h=20$. Circles, squares, and diamonds correspond to $\lambda=0.5$, 1.0, and 2.0, respectively. The reduced shear rate is chosen as $\dot{\gamma}^{*}=0.1$. The solid line denotes the NI model result [4], dashed ($\lambda=0.5$) and dash-dotted ($\lambda=2.0$) lines the DMF model, each for $h\to\infty$.

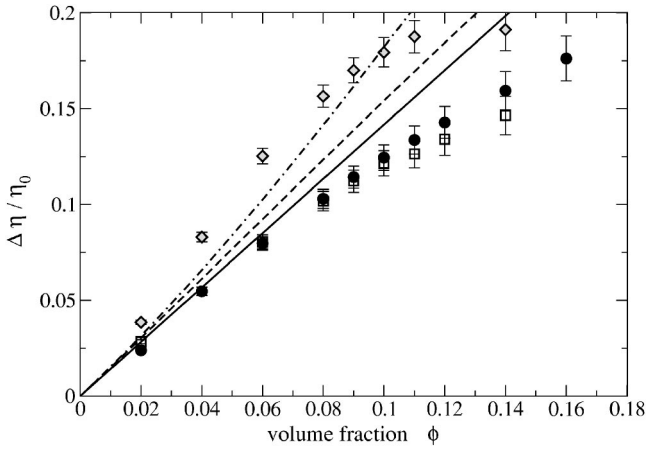

FIG. 10. The relative viscosity change $\Delta\eta/\eta_0-1$ is shown as a function of the volume fraction ϕ. Circles, squares, and diamonds correspond to $\lambda=0.5$, 1.0, and 2.0, respectively. The solid line corresponds to the maximum viscosity increase predicted by the NI model, dashed ($\lambda=0.5$) and dash-dotted ($\lambda=2.0$) lines the maximum viscosity increase predicted by the DMF model.

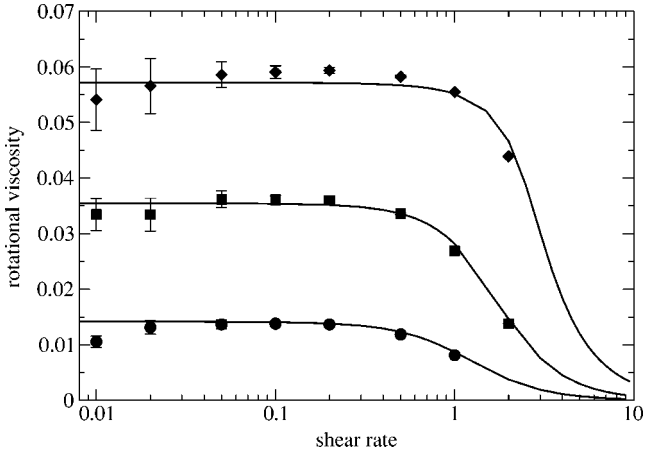

FIG. 11. Rotational viscosity η^*_{rot} as a function of shear rate $\dot{\gamma}^*$. Circles, squares, and diamonds correspond to $h=1.0$, 2.0, and 4.0, respectively. The volume fraction $\phi=0.05$ and dipolar interaction strength $\lambda=1.0$ have been chosen. The solid line corresponds to NI model prediction in the effective field approximation.

netic field. This prediction seems to be well confirmed by the simulation data. In Fig. 9 we show that the DMF model predictions are also in good quantitative agreement. However, we had to use a lower value of the coefficient c_4 in the zero-field viscosity ($c_4\approx 3$) (see Sec. III B), than our simple estimate ($c_4\approx 8.34$) based on a simple form of the pair correlation function. Since the coefficient c_4 is sensitive to details of the pair correlation function, such a discrepancy is to be expected. In Fig. 10, the relative viscosity increase $\Delta\eta/\eta_0$ is shown as a function of the volume fraction ϕ. Here, the viscosity increase is calculated for $h=20$, i.e., from the data shown in Fig. 9. For $\lambda=0.5$, 1.0, the relative viscosity increase is smaller than in the noninteracting case, since η_0 is underpredicted by the NI model (see Fig. 9). For $\lambda=2.0$, however, $\Delta\eta/\eta_0$ is higher than predicted by the NI model, since the maximum viscosity increase overcompensates the increase of η_0. From Figs. 9 and 10 we conclude that predictions of the relative viscosity change based on the NI model benefit from a partial cancellation of terms, neglected in the NI model.

The dependence of the rotational viscosity on the shear rate is depicted in Fig. 11. We observe, that the rotational viscosity stays constant for shear rates $\dot{\gamma}^*<0.5$ and decreases for higher shear rates. Thus, $\dot{\gamma}^*=0.1$ as chosen above, can be considered to be in the weak shear limit, validating previous comparisons to zero-shear results of analytical calculations. The solid line in Fig. 11 shows the prediction of the NI model in the effective field approximation. For the present choice of parameters, $\phi=0.05$, $\lambda=1.0$, the agreement with the simulation results is very good.

4. Normal stress differences

Dimensionless normal stress differences $N_1^*=P_{yy}^*-P_{xx}^*$, $N_2^*=P_{zz}^*-P_{yy}^*$ as a function of the Langevin parameter h are presented in Fig. 12. We observe that N_1 is positive, N_2 is negative, and N_1 and $|N_2|$ increase with increasing h. The field dependence is well described by $N_i\propto L_1^2(h)$ which is predicted by the DMF model. Figure 13 shows the ratio of normal stress differences $-N_2/N_1$ as a function of h. Within the error bars, the ratio $-N_2/N_1$ is found to be independent of h, again in agreement with the predictions of the DMF model. From the simulation results we find $-N_2/N_1\approx 1.0\pm 0.05$ at least for strong magnetic fields where the error bars are small enough, which is slightly lower than 1.17 as predicted by the DMF model. It would be very interesting to compare these findings to experimental results. Unfortunately, however, measurements of the first normal stress difference are rarely reported in the literature and, to the best of our knowledge, the second normal stress difference has been measured only in [28]. From these experiments, one can deduce a single data point for the ratio $-N_2/N_1\approx 0.24$ at mod-

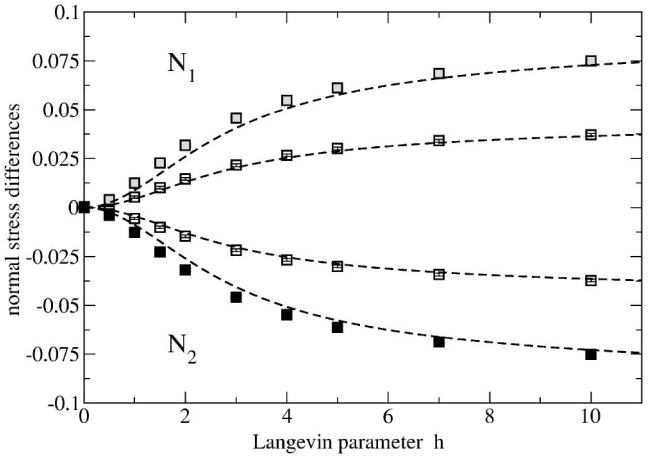

FIG. 12. Reduced normal stress differences N_1^*, N_2^* as functions of the Langevin parameter h. The same flow conditions and parameters as well as the same symbols as in Fig. 4 are used. For better visibility, only $\phi=0.1$ and $\lambda=0.5$ (open symbols) and $\lambda=1.0$ (gray symbols) are shown. The dashed lines are a fit based on the DMF model (see Sec. III).

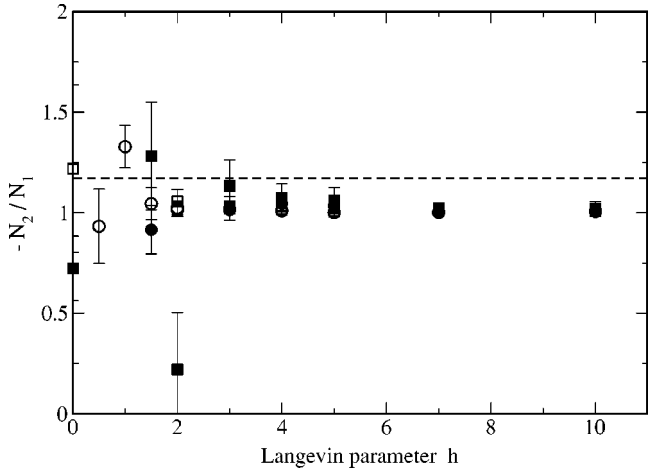

FIG. 13. Ratio of normal stress differences $-N_2/N_1$ as a function of the Langevin parameter h. The same flow conditions and parameters as well as the same symbols as in Fig. 4 are used. The dashed line is the prediction of the DMF model.

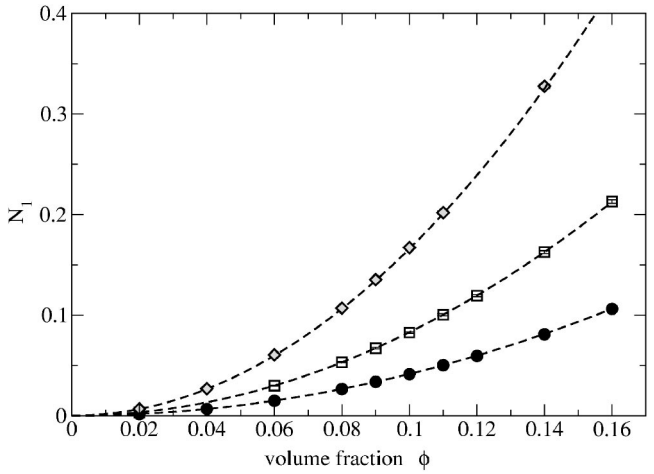

FIG. 14. The first normal stress difference N_1^* as a function of the volume fraction ϕ. Circles, squares, and diamonds correspond to $\lambda=0.5$, 1.0, and 2.0, respectively. The reduced shear rate is chosen as $\dot{\gamma}^*=0.1$. A strong magnetic field $h=20$ is applied in the gradient direction of the flow. The dashed lines are the result of a quadratic fit.

erate magnetic field strengths. This result is compatible with the present results, but further measurements at different magnetic field strengths are needed in order to verify this result.

Finally, the dependence of the first normal stress difference N_1 on the volume fraction ϕ is resolved by the data in Fig. 14. The reduced shear rate is $\dot{\gamma}^*=0.1$ and a large value of the magnetic field $h=20$ is chosen. We observe that the behavior is well described by $N_1 \propto \lambda \phi^2$ as proposed by the mean-field model [9]. The magnitude of the coefficient of proportionality, which depends on the shear rate and magnetic field, however, is much larger than expected from the mean-field model. Further investigations are necessary to elucidate the origin of this difference.

V. CONCLUSIONS

Extensive nonequilibrium molecular simulations have been performed in order to investigate magnetoviscous and viscoelastic effects of ferrofluids. Plane shear flow with the magnetic field oriented in the gradient direction of the flow has been considered. We observe that dipolar interactions increase the equilibrium as well as the nonequilibrium magnetization and the shear viscosity.

For small concentrations ϕ and weak dipolar interactions λ, giving raise to a Langevin susceptibility of $\chi_L=8\lambda\phi \leq 0.5$, the effect of dipolar interactions on the magnetization and shear viscosity is weak enough, such that the results are well described by the kinetic model for noninteracting magnetic dipoles. The dynamical mean-field model proposed recently by two of the authors [9] provides an improvement over the NI model and describes the simulation data even better in this regime. For stronger dipolar interactions, the values of the magnetization and shear viscosity increase more drastically from the predictions of the NI model. Neither the NI nor the DMF model is applicable in this regime and therefore they cannot be expected to give quantitative correct predictions for these parameters. The DMF model may still be of some value under these conditions for a first estimate of the deviations from the NI model. In particular, as a first order model, the DMF model predicts a dependence on χ_L only, but fails to account for the separate dependence on ϕ and λ, which becomes important for higher concentrations or stronger dipolar interactions. These conclusions are similar to those drawn in [15] for the equilibrium magnetization.

For larger concentrations, incorporating dipolar interactions within the DMF model leads to satisfactory agreement with simulation results in the weakly interacting regime. While the nonequilibrium magnetization and magnetoviscous effect are at least qualitatively described by the NI model, the NI model fails to explain the nonlinear increase of the viscosity with volume fraction and the presence of normal stress differences. In particular the field and concentration dependence of the normal stress differences is very well described by the DMF model. Also the prediction that the ratio of the first and second normal stress differences is independent of the magnetic field strength is well confirmed by the simulation results. For strong dipolar interactions, strong cluster formation is observed in the simulations and the DMF model becomes inapplicable. Cluster formation and its relation to viscous properties have been studied in a dipolar system [11], in dense, fully oriented ferrofluids and in magnetorheological fluids (see, e.g., [3,29] and references therein).

We mention, that the NI model can be used to describe also semidilute ferrofluids, if the diameter of the particles is used as a fitting parameter. This procedure is frequently employed in order to fit experimental data on the viscosity of ferrofluids (see Odenbach and Thurm in [1]). The DMF model explains this effective diameter in terms of dipolar interactions. Similarly, strongly interacting ferrofluids might

be described by the DMF model, if the ratio of relaxation times κ is treated as a fitting parameter. This route is not followed in the present study.

Further investigations and comparison to experimental results, in particular for the semidilute regime, are currently being performed. Extensions of the DMF to strong dipolar interactions would be very desirable.

ACKNOWLEDGMENTS

Valuable discussions with S. Odenbach are gratefully acknowledged. P.I. is grateful to Z. Wang for providing his numerical data of Ref. [15]. This work has been performed under the auspices of the DFG-SPP 1104 "Kolloidale magnetische Flüssigkeiten."

[1] *Ferrofluids: Magnetically Controllable Fluids and Their Applications*, edited by S. Odenbach, Lecture Notes in Physics Vol. 594 (Springer, Berlin, 2002).
[2] S. Odenbach, J. Phys.: Condens. Matter **15**, S1497 (2003).
[3] M. Kröger, P. Ilg, and S. Hess, J. Phys.: Condens. Matter **15**, S1403 (2003).
[4] M. A. Martsenyuk, Y. L. Raikher, and M. I. Shliomis, Sov. Phys. JETP **38**, 413 (1974).
[5] S. Odenbach and H. W. Müller, Phys. Rev. Lett. **89**, 037202 (2002).
[6] A. Y. Zubarev and L. Y. Iskakova, Phys. Rev. E **61**, 5415 (2000).
[7] P. Ilg and M. Kröger, Phys. Rev. E **66**, 021501 (2002); **67**, 049901(E) 2003.
[8] P. Ilg, M. Kröger, S. Hess, and A. Y. Zubarev, Phys. Rev. E **67**, 061401 (2003).
[9] P. Ilg and S. Hess, Z. Naturforsch., A: Phys. Sci. **58**, 589 (2003).
[10] H. W. Müller and M. Liu, Phys. Rev. E **64**, 061405 (2001).
[11] J.-J. Weis, J. Phys.: Condens. Matter **15**, S1471 (2003).
[12] A. Satoh, R. W. Chantrell, G. N. Coverdale, and S. Kamiyama, J. Colloid Interface Sci. **203**, 233 (1998).
[13] A. Satoh, R. W. Chantrell, and G. N. Coverdale, J. Colloid Interface Sci. **209**, 44 (1999).
[14] H. Morimoto and T. Maekawa, Int. J. Mod. Phys. B **15**, 823 (2001).
[15] Z. Wang, C. Holm, and H. W. Müller, Phys. Rev. E **66**, 021405 (2002).
[16] W. T. Coffey, Y. P. Kalmykov, and J. T. Waldron, *The Langevin Equation*, Contemporary Chemical Physics, Vol. 11 (World Scientific, Singapore, 1996).
[17] M. P. Allen and D. J. Tildesley, *Computer Simulation of Liquids* (Oxford University Press, Oxford, 1987).
[18] R. G. Larson, *The Structure and Rheology of Complex Fluids* (Oxford University Press, New York, 1999).
[19] P. Ilg, M. Kröger, and S. Hess, J. Chem. Phys. **116**, 9078 (2002).
[20] B. Huke and M. Lücke, Phys. Rev. E **62**, 6875 (2000).
[21] B. U. Felderhof and R. B. Jones, J. Phys.: Condens. Matter **15**, 4011 (2003).
[22] S. Hess, Z. Naturforsch. A **31**, 1034 (1976).
[23] S. Hess, Z. Naturforsch. A **31**, 1507 (1976).
[24] N. A. Clark and B. J. Ackerson, Phys. Rev. Lett. **44**, 1005 (1980).
[25] S. Hess, Phys. Rev. A **22**, 2844 (1980).
[26] J. L. McWhirter and G. N. Patey, J. Chem. Phys. **117**, 2747 (2002).
[27] O. Ambacher, S. Odenbach, and K. Stierstadt, Z. Phys. B: Condens. Matter **86**, 29 (1992).
[28] S. Odenbach, T. Rylewicz, and H. Rath, Phys. Fluids **11**, 2901 (1999).
[29] S. Hess, T. Weider, and M. Kröger, Magnetohydrodynamics **37**, 297 (2001).